Available online at www.sciencedirect.com
ScienceDirect
Geochimica et Cosmochimica Acta 73 (2009) 3201–3217
Geochimica et Cosmochimica Acta
www.elsevier.com/locate/gca

An atomic force microscopy study of calcite dissolution in saline solutions: The role of magnesium ions

E. Ruiz-Agudo [a], C.V. Putnis [b], C. Jiménez-López [c], C. Rodriguez-Navarro [a,*]

[a] Dept. Mineralogía y Petrología, Universidad de Granada, Fuentenueva s/n, 18002 Granada, Spain
[b] Institut für Mineralogie, Universität Münster, Corrensstrasse 24, D-48149 Münster, Germany
[c] Dept. Microbiología, Universidad de Granada, Fuentenueva s/n, 18002 Granada, Spain

Received 24 July 2008; accepted in revised form 17 March 2009; available online 26 March 2009

Abstract

In situ Atomic Force Microscopy, AFM, experiments have been carried out using calcite cleavage surfaces in contact with solutions of $MgSO_4$, $MgCl_2$, Na_2SO_4 and NaCl in order to attempt to understand the role of Mg^{2+} during calcite dissolution. Although previous work has indicated that magnesium inhibits calcite dissolution, quantitative AFM analyses show that despite the fact that Mg^{2+} inhibits etch pit spreading, it increases the density and depth of etch pits nucleated on calcite surfaces and, subsequently, the overall dissolution rates: i.e., from $10^{-11.75}$ mol cm^{-2} s^{-1} (in deionized water) up to $10^{-10.54}$ mol cm^{-2} s^{-1} (in 2.8 M $MgSO_4$). Such an effect is concentration-dependent and it is most evident in concentrated solutions ($[Mg^{2+}] >> 50$ mM). These results show that common soluble salts (especially Mg sulfates) may play a critical role in the chemical weathering of carbonate rocks in nature as well as in the decay of carbonate stone in buildings and statuary.

1. INTRODUCTION

Mineral dissolution plays a central role in a wide range of natural and engineering processes including weathering of minerals and rocks (White and Brantley, 1995; Smith et al., 2000), the deterioration of concrete and building stone (Kanellopoulou and Koutsoukos, 2003), possible mobilization of nuclear wastes (El-Korashy, 2003) and heavy metal release in natural and waste water (García-Sánchez and Álvarez-Ayuso, 2002; El-Korashy, 2003). Investigations of mineral–water interactions and mineral weathering rates are therefore of tremendous interest in many fields. In this respect, the calcite–water system has attracted a significant amount of research due to the abundance of this mineral on the Earth surface and its interest in both biogenic and abiogenic systems. In particular, calcite-solution reactions (growth, dissolution and replacement) are pivotal for a range of processes such as the removal of heavy metals from the environment by adsorption on mineral surfaces (Davis et al., 1987; García-Sánchez and Álvarez-Ayuso, 2002), carbon dioxide sequestration (O'Connor et al., 1999; Wolf et al., 2004; Bearat et al., 2006), carbonate-rocks landscape modeling and evolution (Trenhaile, 1987), the deterioration of building stone (Bell, 1993) and biomineralization (Mann, 2001). There is a voluminous literature regarding calcite dissolution (e.g., see review by Morse and Arvidson, 2002). It is known that calcite dissolution is affected dramatically by the presence of foreign substances both inorganic and organic (Barwise et al., 1990; Morse and Arvidson, 2002; Kanellopoulou and Koutsoukos, 2003). Water in contact with minerals often contains significant amounts of solutes. For example, salt concentration in pore waters of sedimentary rocks varies approximately by five orders of magnitude (Hanor, 1994): from dilute meteoric water to waters with more than 600 g L^{-1} of dissolved salts (Gledhill and Morse, 2006a,b). Additionally, such concentrations may change due to evaporation and condensation phenomena. Alkali and alkaline-earth cations are major components of these aqueous solutions (Morel, 1983). Among them Mg^{2+}, a major

* Corresponding author.
E-mail address: carlosrn@ugr.es (C. Rodriguez-Navarro).

0016-7037/$ - see front matter © 2009 Elsevier Ltd. All rights reserved.
doi:10.1016/j.gca.2009.03.016

cation in sea water, saline lakes and subsurface waters, is known to have an influence on calcite dissolution (Arvidson et al., 2006). Such an influence appears to be pH-dependent. While Alkattan et al. (2002) have reported no effect of Mg^{2+} on calcite dissolution at acid pH, several works have highlighted the role of Mg^{2+} as an inhibitor of calcite dissolution at neutral or moderately alkaline pH in solutions with concentrations below ~80 mM (Berner, 1967; Sjöberg, 1978; Compton and Brown, 1994; Sabbides and Koutsoukos, 1995; Arvidson et al., 2006). However, few publications have focused on the influence of Mg^{2+} in dissolution of calcite at circum-neutral pH and high ionic strength ($[Mg^{2+}] > 50$ mM), conditions that are prevalent in brines and pore waters in sedimentary rocks (Gledhill and Morse, 2006a) as well as in solutions leading to precipitation of magnesium salts such as epsomite ($MgSO_4{\cdot}7H_2O$) within ornamental carbonate stones (Goudie and Viles, 1997; Ruiz-Agudo et al., 2007).

In recent years the study of mineral–water interactions has experienced a significant advance due to the use of *in situ* AFM. This technique has enabled nanoscale observations of mineral surfaces reacting with fluids, as well as real-time studies of the dissolution and precipitation of sparingly soluble minerals, thus facilitating a precise and representative analysis of mineral–water interactions (Hillner et al., 1992; Hall and Cullen, 1995; Putnis et al., 1995; Jordan and Rammensee, 1997; Shiraki et al., 2000; Shtukenberg et al., 2005). The aim of this paper is to present a systematic AFM study of the dissolution of calcite in a range of neutral aqueous solutions containing Mg^{2+} ions with different ionic strength (from 3.2×10^{-5} M to 11.6 M) in order to determine the role played by magnesium in the dissolution of calcite.

2. EXPERIMENTAL

Rhombohedral calcite fragments were cleaved from single crystals of optical quality Iceland spar (Chihuahua, Mexico) with a knife blade. The fragments were examined by optical microscopy to ensure that the cleavage surfaces were free from macroscopic steps and small particles. The calcite $\{10\bar{1}4\}$ surfaces, ca. $3 \times 3 \times 1$ mm in size, were used as substrates and freshly cleaved prior to each experiment.

The calcite $\{10\bar{1}4\}$ faces are F faces, with 3 non-equivalent periodic bond chains (PBC) oriented along $<2\bar{2}1>$, $<\bar{4}41>$ and $<010>$ (Paquette and Reeder, 1995). There are four steps parallel to $<\bar{4}41>$ PBCs: $[\bar{4}41]_+$, $[48\bar{1}]_+$, $[\bar{4}41]_-$ and $[48\bar{1}]_-$ that form the straight edges of the etch pits developed during calcite dissolution (Hillner et al., 1992; Liang and Baer, 1997) or the growth steps developed during calcite growth (Davis et al., 2000). The subscripts (+ or −) follow the convention used by Paquette and Reeder (1995). Steps parallel to the same direction are not structurally equivalent (Astilleros et al., 2006). The structurally equivalent $[\bar{4}41]_-$ and $[48\bar{1}]_-$ steps are acute and intersect the floor of the etch pit at 78° angle, while $[\bar{4}41]_+$ and $[48\bar{1}]_+$ steps are obtuse and intersect the bottom of the etch pit at 102° angle (Hay et al., 2003). The intersection of etch pit edges results in the formation of three kinds of corners: one acute/acute (−/−), one obtuse/obtuse (+/+) and two mixed corners (−/+). This notation will be used here to describe step and etch pit geometry and their evolution.

In situ observations and measurements of the $\{10\bar{1}4\}$ calcite surfaces during dissolution were performed using a fluid cell of a Digital Instruments Nanoscope III Multimode AFM working in contact mode under ambient conditions of both temperature (20 °C) and partial pressure of carbon dioxide ($pCO_2 \approx 10^{-3.5}$ atm). The scanning frequency was 4 Hz, giving an average scan time of 1.5 scans per min and the areas scanned were mostly 5×5 and 10×10 μm. The AFM piezo was calibrated in the x, y and z directions immediately prior to the experimental runs, to ensure accurate voltage to nm conversion. AFM images were collected using Si_3N_4 tips (Veeco Instruments, tip model NP-S20) with spring constants 0.12 N m^{-1} and 0.58 N m^{-1}. Images were analyzed using the NanoScope software (Version 5.12b48).

Measurements of step retreat velocity (or etch pit spreading rate) were made from sequential images scanned in the same direction. The retreat velocity v_{sum} (nm s^{-1}) given by $v_{sum} = (v_+ + v_-)$ (where v_+ and v_- are the retreat velocities of + and − steps, respectively) was calculated measuring the length increase per unit time between opposite parallel steps in sequential images. The ratio v_+/v_- was obtained by measuring the slopes of steep pits as follows (Duckworth and Martin, 2004): $v_+/v_- = m_+/m_-$ were m_+ and m_- are the slopes of the obtuse and acute pit walls, respectively. Knowing v_{sum} and m_+/m_-, v_+ and v_- can readily be calculated. In a few cases, values of v_+ and v_- (as well as v_+/v_-) could be determined by measuring the distance of + and − step edges to fixed points in sequential images (as in Duckworth and Martin, 2004).

Dissolution rates were determined by measuring the volume increase of etch pits, ΔV (cm^3) in time-sequence AFM images of a given area of calcite (density = 2.71 g cm^{-3}; molar volume = 36.93 cm^3 mol^{-1}). During dissolution, etch pits deepen and widen, thus changing their height and lateral dimensions. By measuring depth and area increments of individual etch pits on a given pair of sequential AFM images, as well as etch pit density (calculated by digital image analysis in terms of fractional area occupied by etch pits), dissolution rates, R_{AFM} (mol cm^{-2} s^{-1}) were obtained using the equation:

$$R_{AFM} = x_A \frac{\Delta V}{A V_m t} \quad (1)$$

where ΔV is the volume increment of a given etch pit, A (cm^2) is the surface area of the etch pit, x_A is the fractional area occupied by all etch pits in a given image, t (s) is the time interval between sequential images, and V_m is the molar volume of calcite. Note that sufficiently large images (i.e., scan area $\geqslant 25$ μm^2) are required for x_A values to be representative. Otherwise, an overestimation of x_A and, as a consequence, R_{AFM} may occur. For instance, if the whole image is occupied by a single etch pit (i.e., $x_A = 1$), rates will typically be about one order of magnitude higher than those determined when typical (observed) x_A values of 0.1–0.45 are considered. Average R_{AFM} values (and standard deviations) were obtained from the analysis of at least six etch pits in three pairs of sequential images of a given

run. Although tedious and time-consuming, this procedure enables calculation of surface area-specific dissolution rates from AFM measurements (Dove and Platt, 1996; Shiraki et al., 2000; Duckworth and Martin, 2004). However, this calculation has some limitations. First, due to the absence of a reference (unreacted) surface on the mineral, the measurements were only realistic in the cases where layer removal was slower than the increase in etch pit depth (i.e., experiments with salt concentration above 0.3 mM where deep etch pits formed). In order to minimize the influence of layer removal, etch pit lateral spreading and depth measurements were only performed using successive images where no fast retreating steps formed at intersecting shallow pits. Dissolution rates obtained using such etch pits are still valid because rates are roughly similar in both deep etch pits and areas with high velocity steps at intersecting pits (Jordan and Rammensee, 1998). On the other hand, it should be noted that, under similar experimental conditions (i.e., far from equilibrium, circum-neutral pH, room T and P), dissolution rates determined using AFM are typically about one order of magnitude smaller than those determined from "bulk" powder experiments (Arvidson et al., 2003) as well as those determined from total calcium measured in the AFM fluid-cell effluent solution (Duckworth and Martin, 2004). According to Arvidson et al. (2003) this discrepancy is explained by the high density of kinks and steps at grain boundaries (not taken into account during AFM measurements) that contributes to enhanced "bulk" dissolution rates. Finally, and regarding the validity of dissolution rates determined using AFM, note that Dove and Platt (1996) have shown that this type of AFM measurements leads to realistic calcite dissolution rates when values are in the range 10^{-14} to 10^{-10} mol cm^{-2} s^{-1} (i.e., within the range observed here).

Calcium-free saline solutions in concentrations ranging from 0.01 mM to saturation (with respect to the saline phase) flowed continuously for 30 min at 50 mL h^{-1} from a syringe coupled to an O-ring-sealed fluid cell containing the sample crystal. We have employed sufficiently high flow rates to measure dissolution rates that are surface controlled. As pointed out by Arvidson et al. (2006), this strategy is consistent with many of the published AFM experiments that address both calcite dissolution (e.g., Liang et al., 1996) and growth (e.g., Teng et al., 1998). For instance, Liang et al. (1996) have demonstrated that flow rates above 9 mL h^{-1} guarantee that the dissolution process is surface controlled rather than diffusion controlled at slightly alkaline pH, while Shiraki et al. (2000) have observed that for pH > 5.3 the velocity of step retreat is independent of flow rate for values higher than 29 mL h^{-1} (at room T and $pCO_2 \approx 10^{-3.5}$ atm). Note that mass transport is typically an issue at acid pH while, in general, surface reaction kinetics control calcite dissolution in far from equilibrium (i.e., high undersaturation) conditions at circum-neutral or slightly alkaline pH (Arvidson et al., 2003), conditions that are prevalent in our experiments.

Before each dissolution experiment, deionized water and standard growth solution (0.3 mM $CaCl_2$ and Na_2CO_3 giving a saturation index, SI (SI = log Ω = log(IAP/Ksp); where Ω is the saturation state of the system, IAP is the ion activity product and Ksp is the thermodynamic solubility product of the relevant phase) of 0.81 with respect to calcite, calculated using PHREEQC (Parkhurst and Appelo, 1999)) were passed over the crystal to clean the cleaved surface, as well as to adjust the AFM parameters as in Arvidson et al. (2006). In order to single out the role of cations (i.e., Mg^{2+}) and anions (i.e., SO_4^{2-}) in calcite dissolution at the nanoscale, four saline systems were used in the *in situ* AFM dissolution experiments: $MgSO_4$, Na_2SO_4, $MgCl_2$ and NaCl. Solutions were prepared from high-purity Na_2CO_3, $CaCl_2$, $MgSO_4{\cdot}7H_2O$, Na_2SO_4, $MgCl_2$ and NaCl (Panreac, reagent grade) dissolved in deionized water (conductivity < 18 mΩ cm^{-1}). Prior to dissolution experiments, saline solutions were let to equilibrate with ambient atmosphere. In all cases, saline solution pH values were close to neutrality. Table 1 shows experimental conditions for each saline solution, including pH, ion activities, distribution of ionic species, total alkalinity, ionic strength (IS) and SI with respect to either magnesite ($MgCO_3$) and hydromagnesite ($4MgCO_3{\cdot}Mg(OH)_2{\cdot}4H_2O$), or sodium (bi)carbonate phases calculated using the latest version of PHREEQC, which includes Davies equation for diluted solutions and Pitzer equations for concentrated (>0.1 M) solutions (i.e., the pitzer.dat database was used). The EQPITZER code (He and Morse, 1993) which is specific for concentrated saline solutions was also used. Little differences were found, however, between ion activities calculated using both computer codes for concentrations >0.1 M. Thus, we choose to report here only the values calculated with PHREEQC (which also yields reliable values for the solutions with concentrations <0.1 M). Fig. 1 represents calculated distribution of dissolved ionic species as a function of salt concentration in Ca-free saline solutions, as well as values of SI with respect to magnesite (log $Ksp_{\text{magnesite}} = -8.03$; Drever, 1997) and hydromagnesite (log $Ksp_{\text{hydromagnesite}} = -36.769$; Drever, 1997) (Figs. 1a and b) or nahcolite ($NaHCO_3$; log $Ksp_{\text{nahcolite}} = -0.39$; Monnin and Schott, 1984) (Figs. 1c and d). Note that only SI values with respect to nahcolite are presented in Fig. 1 and Table 1, because these values are (some orders of magnitude) higher than those of other sodium carbonate phases such as trona ($Na_3(CO_3)(HCO_3){\cdot}2H_2O$), natron ($Na_2CO_3{\cdot}10H_2O$), or thermonatrite ($Na_2CO_3{\cdot}H_2O$). For similar reasons, SI values for nesquehonite ($MgCO_3{\cdot}3H_2O$) and lansfordite ($MgCO_3{\cdot}5H_2O$) are not presented. The absence of calcium in the saline solutions ensured constant far-from-equilibrium conditions (i.e., high undersaturation) with respect to calcite during *in situ* AFM experiments: i.e., because the total calcium in the saline solutions is zero, $\Omega = 0$ and SI $\rightarrow -\infty$. Each experiment was repeated 3 times to test reproducibility.

After flowing through the fluid cell, 20 mL aliquots of effluent solution were collected for calcium analysis by inductively coupled plasma optical emission spectrometry, ICP-OES (Atom Scan 25 Thermo Jarrell Ash). Macroscopic dissolution rates of calcite, R_{mac} (mol cm^{-2} s^{-1}) were calculated as follows:

$$R_{mac} = \frac{Ca_T Q}{A} \quad (2)$$

Table 1
Experimental and calculated parameters for the inlet saline solutions.

$MgSO_4$ conc. (mM)	pH	$SI_{magnesite}$	$SI_{hydromagnesite}$	Total alkalinity (eq L^{-1})	Ionic strength (M)	Ionic species (M)					
						$aMgCO_3^\circ$	aMg^{2+}	aCO_3^{2-}	$aHCO_3^-$	$aHSO_4^-$	aSO_4^{2-}
0.01	6.9	−7.33	−28.54	−4.65E−08	0.00004	3.68E−13	9.69E−06	4.48E−11	2.20E−06	2.08E−09	9.69E−06
0.05	6.9	−6.64	−25.80	−4.69E−08	0.0002	1.78E−12	4.67E−05	4.50E−11	2.21E−06	9.98E−09	4.67E−05
0.3	7.1	−5.74	−21.88	5.21E−08	0.0012	1.02E−11	3.00E−04	5.60E−11	2.28E−06	5.24E−08	2.53E−04
1	6.8	−5.43	−21.17	3.98E−08	0.004	2.89E−11	7.29E−04	4.68E−11	2.25E−06	1.53E−07	7.28E−04
10	7	−4.54	−17.32	3.39E−07	0.04	2.27E−10	4.30E−03	6.24E−11	2.60E−06	7.25E−07	4.00E−03
50	7.1	−3.91	−14.76	3.34E−07	0.20	9.60E−10	1.28E−02	8.84E−11	3.09E−06	1.51E−06	9.90E−03
100	7	−3.67	−14.03	2.61E−06	0.40	1.68E−09	2.02E−02	9.83E−11	3.26E−06	1.96E−06	1.36E−02
500	7.1	−3.01	−11.37	−1.06E−07	2.00	7.56E−09	6.44E−02	1.39E−10	3.85E−06	2.70E−06	2.22E−02
1000	7.1	−2.67	−10.04	5.90E−06	4.00	1.67E−08	1.29E−01	1.53E−10	4.03E−06	2.64E−06	2.30E−02
2900	7	−1.45	−5.47	3.98E−05	11.60	2.77E−07	1.68E+00	1.95E−10	4.38E−06	1.38E−06	1.40E−02

$MgCl_2$ conc. (mM)	pH	$SI_{magnesite}$	$SI_{hydromagnesite}$	Total alkalinity (eq L^{-1})	Ionic strength (M)	$aMgCO_3^\circ$	aMg^{2+}	aCO_3^{2-}	$aHCO_3^-$	aCl^-
0.01	6.9	−7.33	−28.53	−4.63E−08	0.00003	3.69E−13	9.74E−6	4.48E−11	2.20E−06	1.99E−05
0.05	7	−6.63	−25.56	1.21E−09	0.00015	1.83E−12	4.72E−5	4.57E−11	2.22E−06	9.86E−05
0.3	7.1	−5.88	−22.35	5.41E−08	0.0009	1.04E−11	2.62E−4	4.68E−11	2.25E−06	5.80E−04
1	6.98	−5.41	−20.70	3.47E−09	0.003	3.06E−11	7.91E−4	4.57E−11	2.22E−06	1.88E−03
10	7.3	−4.52	−16.58	3.77E−07	0.03	2.35E−10	5.41E−3	5.11E−11	2.35E−06	1.69E−02
50	7.3	−3.98	−14.41	8.95E−07	0.15	8.27E−10	1.82E−2	5.35E−11	2.40E−06	7.38E−02
100	7.1	−3.81	−14.06	8.11E−07	0.30	1.22E−09	3.14E−2	4.60E−11	2.23E−06	1.37E−01
500	7	−3.13	−11.51	2.67E−06	1.50	5.85E−09	1.61E−1	4.28E−11	2.12E−06	5.82E−01
1000	6.9	−2.37	−8.88	6.79E−06	3.00	3.36E−08	5.70E−1	6.97E−11	2.66E−06	1.136
2000	7.2	0.10	0.19	1.16E−04	6.00	1.02E−05	6.23E+0	1.92E−09	1.02E−05	2.441

Na_2SO_4 conc. (mM)	pH	$SI_{Nahcolite}$	Total alkalinity (eq L^{-1})	Ionic strength (M)	Ionic species (M)				
					aNa^+	$aHCO_3^-$	aCO_3^{2-}	$aHSO_4^-$	aSO_4^{2-}
0.01	7	−9.95	3.6E−10	0.00003	0.000019	2.24E−06	4.58E−11	2.07E−−09	9.74E−06
0.05	6.8	−9.27	−9.73E−08	0.00015	9.86E−05	2.18E−06	4.40E−11	4.72E−05	1.02E−08
0.3	7.1	−9.22	4.65E−08	0.0009	5.79E−04	2.27E−06	4.78E−11	5.44E−08	2.62E−04
1	6.85	−7.97	−8.65E−08	0.003	1.88E−03	2.27E−06	4.76E−11	1.64E−07	7.89E−04
10	6.9	−6.95	−1.32E−07	0.03	1.68E−02	2.67E−06	6.61E−11	9.16E−07	5.19E−03
50	6.95	−6.22	−2.57E−07	0.15	7.21E−02	3.34E−06	1.04E−10	2.08E−06	1.48E−06
100	7	−5.91	−3.14E−07	0.30	1.32E−01	3.71E−06	1.28E−10	2.70E−06	2.14E−02
500	7.1	−5.25	−4.82E−07	1.50	5.10E−01	4.36E−06	1.79E−10	4.10E−06	3.69E−02
1000	6.88	−5.02	−1.25E−06	3.00	8.97E−01	4.23E−06	1.71E−10	4.61E−06	4.28E−02
1900	7	−4.67	−9.60E−07	5.70	2.30	3.67E−06	1.36E−10	4.77E−06	4.22E−02

NaCl conc. (mM)	pH	$SI_{Nahcolite}$	Total alkalinity (eq L^{-1})	Ionic strength (M)	aNa^+	$aHCO_3^-$	aCO_3^{2-}	aCl^-
0.01	6.9	−10.2	−4.63E−08	0.000012	9.96E−06	2.20E−06	4.48E−11	9.96E−06
0.05	7	−9.56	4.69E−10	0.000052	4.96E−05	2.22E−06	4.57E−11	4.96E−05
0.3	6.8	−8.79	−9.70E−08	0.0003	2.94E−04	2.18E−06	4.38E−11	2.94E−04
1	6.8	−8.28	−9.85E−08	0.001	9.65E−04	2.17E−06	4.37E−11	9.65E−04
5	7	−7.59	−4.93E−08	0.005	4.64E−03	2.19E−06	4.45E−11	4.63E−03
20	6.9	−7.02	−5.12E−08	0.02	1.75E−02	2.18E−06	4.39E−11	1.74E−02
50	7.3	−6.63	1.87E−07	0.05	4.13E−02	2.24E−06	4.67E−11	4.07E−02
100	7.1	−6.37	6.80E−08	0.10	7.86E−02	2.15E−06	4.28E−11	7.67E−02
500	7	−5.78	3.84E−08	0.50	3.56E−01	1.86E−06	3.24E−11	3.24E−01
1000	7.2	−5.53	2.13E−07	1.00	7.12E−01	1.64E−06	2.58E−11	6.03E−01
5700	7.1	−5.06	2.72E−07	5.70	8.51	4.08E−07	1.99E−12	3.44

where Ca_T is the total calcium in the effluent solution (mol L^{-1}), Q is the solution flow rate (L s^{-1}) and A is the geometric area of calcite exposed to the solution (cm^2). Uncertainties in determining A (i.e., assuming that the calcite is atomically flat) contribute to significant error in R_{mac} determinations (De Giudici, 2002), typically leading to an overestimation of macroscopic dissolution rates (Duckworth and Martin, 2004). Here, the error in A values was estimated to be ±37%. Another source of error is the very low value of Ca_T (a few mmol L^{-1}) in the effluent solution (Arvidson et al., 2006) and the effect of other ions (Mg^{2+} or Na^+) in concentrated saline solutions that preclude obtaining reliable Ca_T concentration results. Thus, here we will present a few selected R_{mac} values only for comparison purposes.

Selected Iceland spar crystals subjected to dissolution tests were analyzed on a Philips PW-1547 X-ray diffractometer with an automatic slit, Cu Kα radiation ($\lambda = 1.5405$ Å), 27° to 33°2θ explored area, with steps of 0.005°2θ and 4 s counting time (static mode). XRD analyses were performed before and after dissolution in water and 2.9 M $MgSO_4$ solution. Following dissolution runs, crystals were gently rinsed with deionized water and ethyl alcohol, dried at room T, and placed in the diffractometer chamber with their $\{10\bar{1}4\}$ cleavage plane parallel to the sample holder. The XPowder software package (Martin-Ramos, 2004) was used for 104 peak broadening analysis and crystallite size determination. This software performs background subtraction and $K\alpha_2$ stripping, and allows implementation of instrumental broadening correction and peak profile fitting (convolution with Gaussian, Lorentzian and/or pseudo-Voight functions), yielding crystallite size using the Scherrer equation. XRD analyses were aimed at determining whether the dissolution altered the crystallinity of the exposed calcite surface either by (random) ion incorporation (i.e., formation of poorly-ordered Mg-calcite) or by annealing of defects. A full scan (from 3° to 70°2θ) was also performed for each run in order to detect possible newly-formed phases.

Iceland spar samples subjected to dissolution were studied with an environmental scanning electron microscope (ESEM, FMI Quanta 400) equipped with EDS microanalysis. No sample preparation (i.e., no C or Au coating) was required for ESEM-EDS analysis.

3. RESULTS

3.1. General features of etch pits

AFM images showed calcite dissolution via etch pit formation 2 min after the injection of deionized water into the fluid cell (Fig. 2a). Dissolution pits (etch pit density ~ 1.2×10^8 cm^{-2}) were shallow, mono and dimolecular steps approx. 3–6 Å in depth and displayed the typical rhombohedral shape that has been thoroughly described (Arvidson et al., 2006 and refs. therein). Typically, the larger shallow pits contained smaller ones (Fig. 2a). In addition to the abundant shallow pits, a few deep pits (density of ~4×10^6 cm^{-2}) with inverted pyramid morphology were

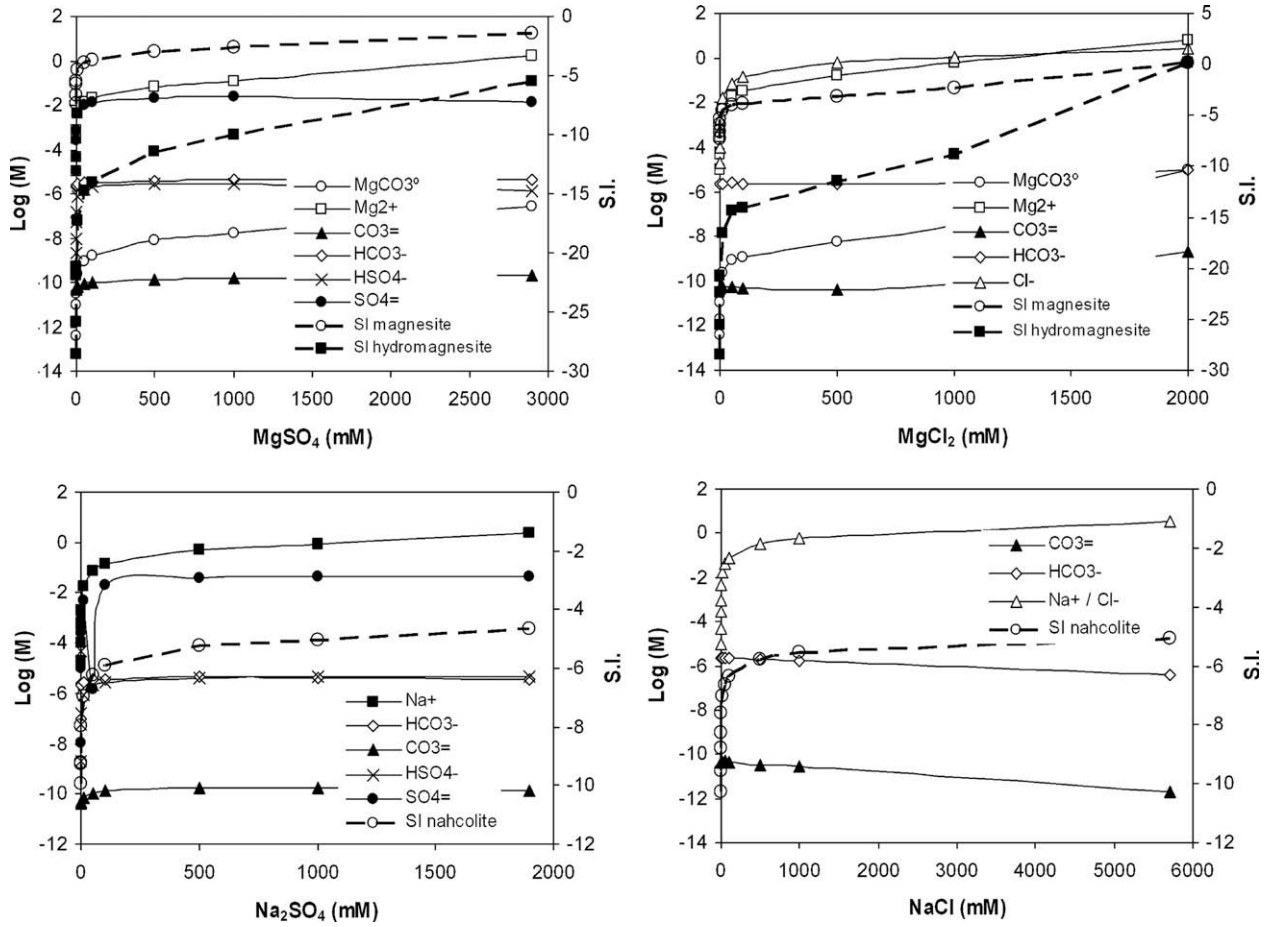

Fig. 1. Calculated distribution of dissolved species vs. salt concentration for the four tested saline solutions. The variation of saturation index (SI) for Mg or Na carbonates (magnesite, hydromagnesite or nahcolite) vs. salt concentration is also shown. Note that with the exception of the saturated (1.9 M) $MgCl_2$ solution, all systems are undersaturated with respect to these carbonate phases.

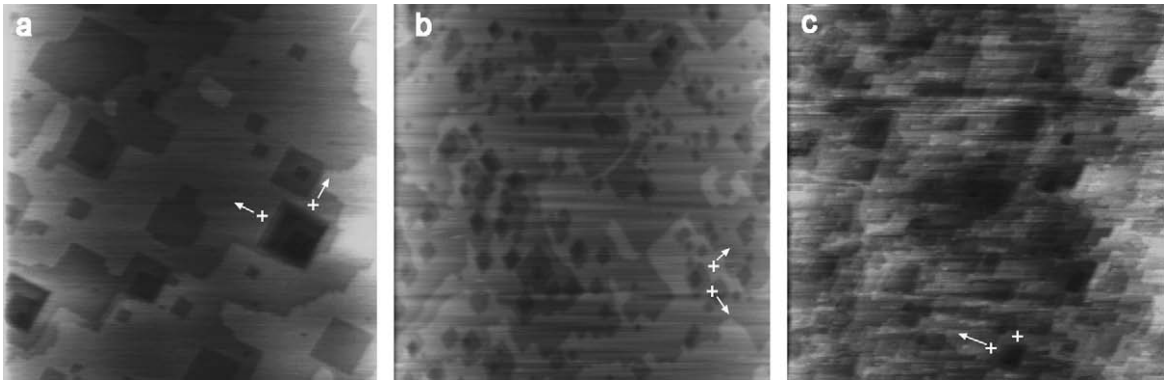

Fig. 2. AFM height images of calcite $\{10\bar{1}4\}$ surfaces after 2 min in contact with flowing: (a) deionized water, (b) 0.03 mM and (c) saturated (2.9 M) $MgSO_4$ solutions. Image size: 5×5 μm. The direction of + steps retreat is indicated (arrows).

present (Fig. 2a). Such deep pits are commonly associated with dislocations outcropping at the calcite surface (MacInnis and Brantley, 1992). We observed that increasing Mg^{2+} concentration led to a general increase in etch pit depth and density (Figs. 2b–c and 3b). In the presence of Na^+, no significant difference was observed in etch pit density or depth if compared with dissolution in deionized water, and the dissolution took place mainly as a layer-by-layer process following intersection of shallow etch pits (Fig. 3a). The calcite etch pit density in saturated (2.9 M) $MgSO_4$ solution was 2.5×10^9 cm^{-2}, a value ~20 times higher than that observed in water or Na sulfate solutions (Fig. 4). Etch pit density was reduced in the presence of Cl^- compared with SO_4^{2-}, although in both cases higher etch pit density values were reached in the presence of Mg^{2+} than in the presence of Na^+.

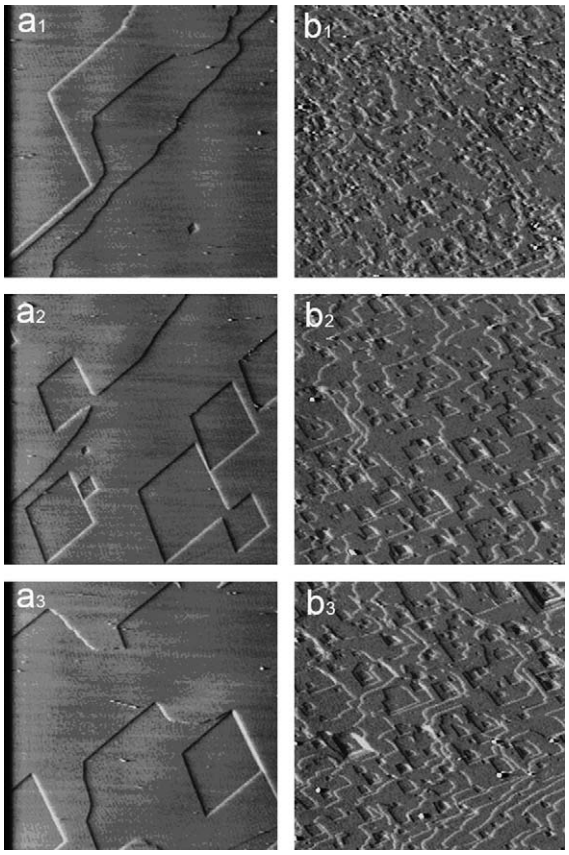

Fig. 3. AFM time sequence (deflection images taken at 2 min intervals) of calcite dissolution in: (a) 1 M Na_2SO_4 and (b) 1 M $MgSO_4$ solutions (Image size: 5 × 5 μm).

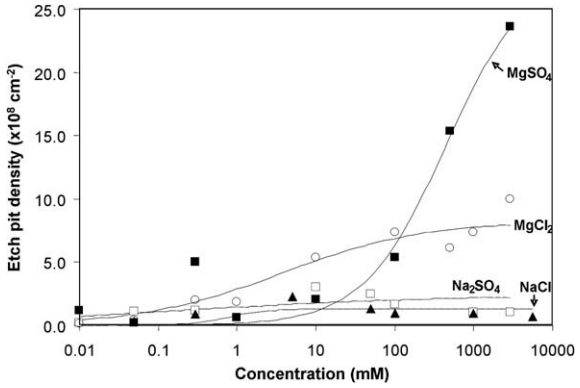

Fig. 4. Salt concentration vs. etch pit density developed on calcite $\{10\bar{1}4\}$ surfaces in contact for 2 min with (■) $MgSO_4$, (□) Na_2SO_4, (○) $MgCl_2$ and (▲) NaCl solutions. Data were adjusted to empiric sigmoidal curves ($y = v_{\max}\frac{x^n}{k^n+x^n}$).

The morphology of etch pits developed in the presence of NaCl and Na_2SO_4 was very similar to that of etch pits developed in the presence of water; i.e., no corner rounding was observed (Figs. 3a and 5a). Conversely, rounding of the +/+ corner of etch pits was systematically observed following dissolution in the presence of Mg^{2+} (Figs. 2c, 3b and 5b). Rounding of +/+ corners was more significant in $MgCl_2$ that in $MgSO_4$ solutions of equal concentration (e.g., compare Figs. 3b and 5b). Upon +/+ corner rounding, the side-walls of etch pits formed by + steps were steeper than those on the opposite side (i.e., the spacing of + steps was << than that of − steps).

Fig. 6a shows a detail of a deep etch pit with straight sides formed in the presence of water. Following exposure to standard growth solution a flat surface was generated upon refilling of the pit. Afterwards, the same area was exposed to 1 M $MgSO_4$ solution, leading to the formation of the etch pit with a rounded +/+ corner depicted in Fig. 6b. In addition to the effect of Mg^{2+} on the etch pit morphology, Figs. 6a and b also show that a dislocation outcropping at the crystal surface (and going to a depth of at least ~3 nm; i.e., the pit depth in Fig. 6c) favored the nucleation of the etch pit and afterward controlled the growth (filling of the pit) and re-dissolution of this specific area. Otherwise, formation of new etch pits on this area should have occurred randomly (MacInnis and Brantley, 1992). Apparently, magnesium-induced changes in the shape of etch pits do not seem to depend on whether etch pits where shallow or deep.

3.2. Etch pit spreading rates

The average velocity of etch pit spreading, v_{sum} (i.e., the rate of change in etch pit length along $[\bar{4}41]$ or $[48\bar{1}]$, thus accounting for the summed retreat of opposite + and − steps) in deionized water was 1.95(±0.5) nm s^{-1} (Fig. 7). The average v_+/v_- ratio was 2.8(±0.4), a value slightly higher than the typical v_+/v_- ratios (determined in pure water) that range from 1.5 to 2.3 (Lea et al., 2001). Note however, that higher ratios of 3.1–5.4 have been reported for similar Iceland spar crystals from Chihuahua, Mexico (Harstad and Stipp, 2007). The average values of v_+ and v_- in deionized water were 1.44(±0.3) nm s^{-1} and 0.51(±0.2) nm s^{-1}, respectively. These values are in good agreement (within experimental error) with those reported by Harstad and Stipp (2007).

At low magnesium concentrations (up to 0.01 mM $MgSO_4$), v_{sum} increased up to 2.87(±0.33) nm s^{-1}. However, upon further increase in the concentration of Mg^{2+} up to 100 mM, v_{sum} was reduced to 0.78(±0.19) nm s^{-1}, a value far below that of deionized water and in good agreement with the value ($v_+ + v_-$) of 0.78(±0.08) nm s^{-1} reported by Arvidson et al. (2006) for calcite dissolution in 0.8 mmolal Mg^{2+}. From 100 mM $MgSO_4$ to saturation (2.9 M $MgSO_4$), spreading rates remained nearly constant and the observed values were systematically below those of deionized water. In the presence of high Mg^{2+} concentrations ($[Mg^{2+}] > 50$ mM), v_+/v_- ratios were significantly reduced (average of 0.32±0.08). For instance, dissolution in 1 M $MgSO_4$ led to a v_+/v_- ratio of 0.38±0.1, where $v_+ = 0.21(\pm0.05)$ nm s^{-1} and $v_- = 0.56(\pm0.14)$ nm s^{-1}. These results show that Mg^{2+} selectively affected (reduced) the retreat velocity of + steps, leading to +/+ corner rounding (as reported by Arvidson et al., 2006). A similar trend was observed in the case of $MgCl_2$ (Fig. 7), where values of v_{sum} smaller than those of deionized water were observed at concentrations as low as 0.05 mM. In contrast, Na^+

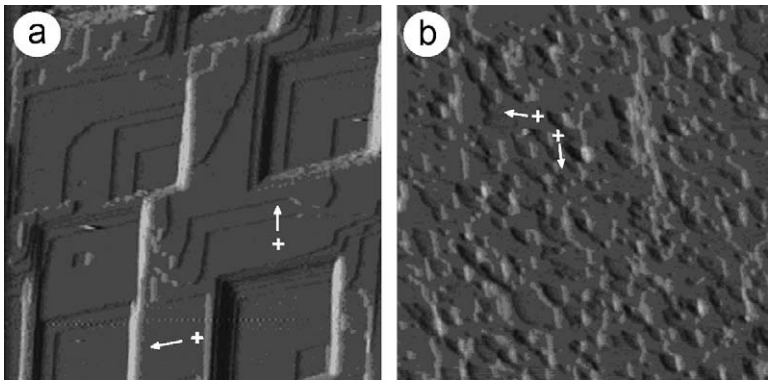

Fig. 5. AFM deflection images of etch pits formed on calcite {$10\bar{1}4$} surfaces after 2 min flowing with (a) 1 M NaCl and (b) 1 M $MgCl_2$ solutions (Image size: 5 × 5 μm). The direction of + steps retreat is indicated (arrows).

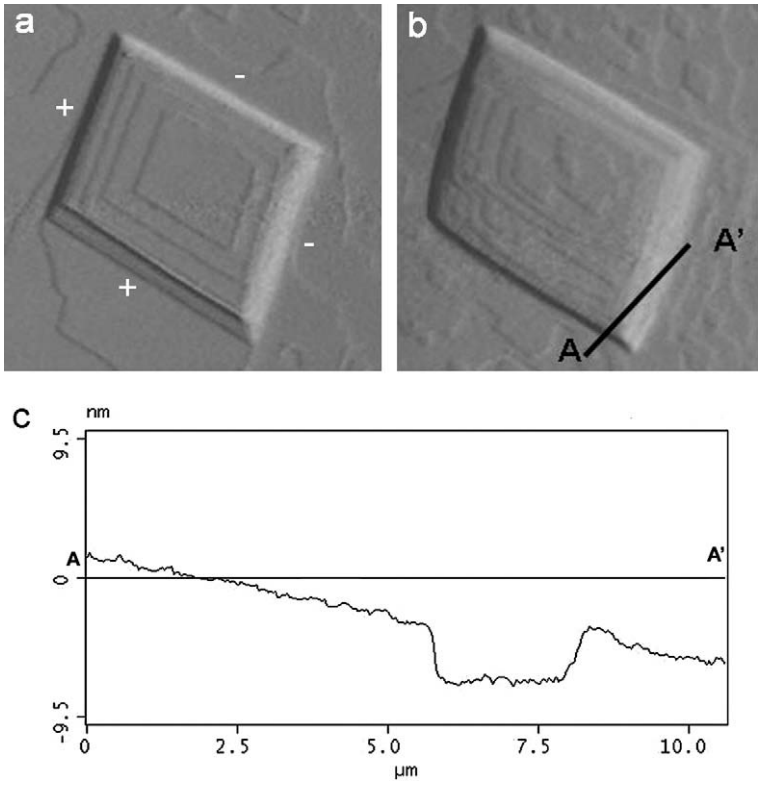

Fig. 6. AFM deflection images of etch pit shape upon dissolution by water (a), and dissolution by 1 M $MgSO_4$ (b); (c) depth profile in section AA′ of the corresponding height image of the etch pit showing a vertical wall in the +/+ section and an oblique wall towards the −/− corner.

showed a reverse trend: v_{sum} increased as the concentration of NaCl or Na_2SO_4 increased (Fig. 7), and v_+/v_- ratios remained unchanged. The latter shows that sodium salts affected (increased) equally the retreat velocity of + and − steps.

3.3. Etch pit deepening rates

We observed an increase in the average rate for etch pit deepening (i.e., rates of surface-normal retreat) from dilute $MgSO_4$ solutions up to 50 mM (Fig. 8a). This trend was reversed at higher concentrations (Fig. 8b). The increase in the deepening rate was however higher than that of water. Similar trends were observed in the case of $MgCl_2$ solutions, although deepening rates were about 25% lower than in the case of $MgSO_4$. Interestingly, for Mg^{2+} concentrations in the range 0.01–0.3 mM, increases in deepening rates were negative (Fig. 8a). The latter implies that whole layers of calcite are eliminated once etch pits start to develop and coalesce, as was observed with the AFM. In this case, we observed fast retreating rough steps similar to those reported by Vinson and Luttge (2005) and Arvidson et al. (2006). Such a layer-by-layer dissolution pattern is similar to that of deionized water and resulted in flat calcite crystal

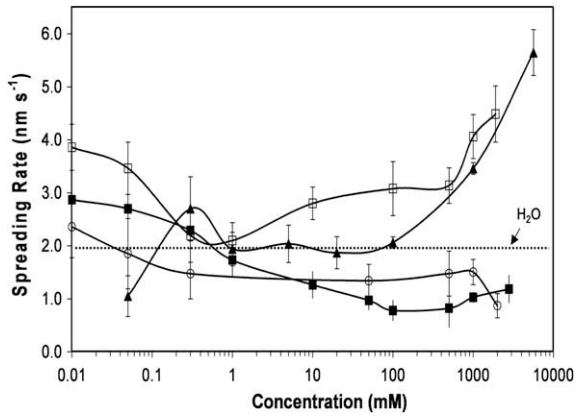

Fig. 7. Average spreading rate of etch pits nucleated on calcite $\{10\bar{1}4\}$ terraces vs. concentration of (■) $MgSO_4$, (○) $MgCl_2$, (□) Na_2SO_4, and (▲) NaCl solutions.

surfaces, in contrast with the rough surfaces developed in the presence of concentrated Mg^{2+} solutions. At Mg^{2+} concentrations higher than 0.3 mM, layer removal was slower than the increase in etch pit depth. This resulted in the observed deepening of the etch pits. Typically, such a deepening was associated with the formation of successive etch pits within preexisting ones, as shown by the AFM image sequence in Fig. 3b. Note, however, that deepening of some etch pits was associated with the retreat of steps emerging from dislocations as shown in Fig. 6.

3.4. Dissolution rates

ICP-OES measurements revealed that the Ca_T concentration in effluent solution increased continuously with Mg^{2+} concentration (up to 1 M Mg^{2+}; at higher concentrations, a significant scattering in $[Ca^{2+}]$ values was observed and these results were therefore discarded) (Table 2). Fig. 9 and Table 2 show values of $\log R_{mac}$ calculated from measured Ca_T values using Eq. (2). The calculated $\log R_{mac}$ for deionized water was $-9.07(\pm0.16)$ mol cm^{-2} s^{-1}. Values of $\log R_{mac}$ followed a nearly exponential increase with magnesium concentration (in the inlet solution) from $-9.07(\pm0.16)$ to $-8.12(\pm0.16)$ mol cm^{-2} s^{-1} ($MgSO_4$ concentrations >1 mM). In addition to the error associated with the estimation of geometric surface area (see Section 2), dissolution rates for $MgSO_4$ concentrations <10 mM (as well as for deionized water) are not highly reliable due to the very low calcium concentration in the effluent

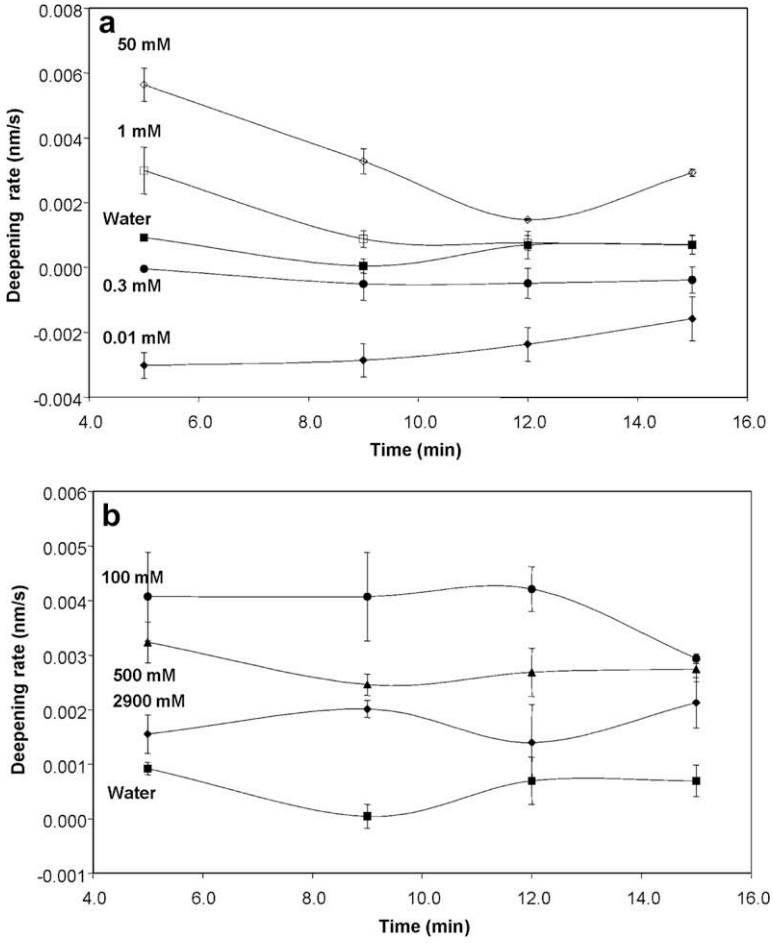

Fig. 8. Average rate of etch pit deepening during dissolution of calcite in the presence of flowing $MgSO_4$ solutions with (a) low concentration (<50 mM) and (b) high concentration (>50 mM).

Table 2
Total calcium concentration, Ca_T in effluent magnesium sulfate solutions and calculated calcite macroscopic dissolution rates, R_{mac} (mol cm^{-2} s^{-1}).

$MgSO_4$ (mM)	Ca_T (mM)	$-\log R_{mac}$
0	0.02(±0.001)	9.07(±0.16)
0.01	0.019(±0.001)	9.10(±0.16)
0.05	0.02(±0.001)	9.07(±0.16)
0.3	0.03(±0.003)	8.90(±0.16)
1	0.02(±0.001)	9.07(±0.16)
10	0.04(±0.002)	8.77(±0.16)
50	0.08(±0.004)	8.47(±0.16)
100	0.1(±0.014)	8.37(±0.18)
500	0.12(±0.002)	8.29(±0.16)
1000	0.18(±0.010)	8.12(±0.16)

solution (i.e., $Ca_T < 0.05$ mM). Hence, values reported in Fig. 9 are only presented as an indication of the trend followed by calcite dissolution rates with increasing magnesium concentration. Nonetheless, the lowest $\log R_{mac}$ observed here approaches the log rate of −9.5 mol cm^{-2} s^{-1} reported by Shiraki et al. (2000). The latter value was determined by Ca_T analysis of AFM fluid-cell effluent solution following Iceland spar dissolution in water at circum-neutral pH and at room T and pCO_2.

Fig. 10 and Table 3 show calcite dissolution rates ($\log R_{AFM}$) calculated from AFM measurements according to Eq. (1). The log rate of calcite dissolution in deionized water was found to be −11.75(±0.18) mol cm^{-2} s^{-1}. This value is comparable to, but slightly lower than the −11.68 mol cm^{-2} s^{-1} "global" surface retreat rate reported by Arvidson et al. (2003) or the −11.10 mol cm^{-2} s^{-1} rate published by Vinson and Luttge (2005), both determined using vertical scanning interferometry. In general, the dissolution rate increased with solute concentration for all four salts tested. At high solute concentration, the dissolution rate was more than one order of magnitude higher in the presence of 2.8 M $MgSO_4$ ($\log R_{AFM} = -10.54(\pm0.05)$ mol cm^{-2} s^{-1}) than in the presence of deionized water. The electrolytes tested increase R_{AFM} in the order $MgSO_4 > MgCl_2 > Na_2SO_4 > NaCl > H_2O$. This trend is in agreement with the observed trend in etch pit formation and deepening. Note, however, that the log rate of calcite dissolution in 10 mM $MgCl_2$ solution reached a minimum value of −12.02(±0.18) mol cm^{-2} s^{-1}. This minimum value confirms that magnesium inhibits the dissolution of calcite at $[Mg^{2+}] < 50$ mM, as has been shown elsewhere (e.g., Compton and Brown, 1994). However, dissolution rates significantly increase at higher Mg^{2+} concentrations in parallel with the increase in etch pit density/deepening and in spite of the observed reduction in etch pit spreading rates. These two critical –and opposite- effects are discussed in Section 4.

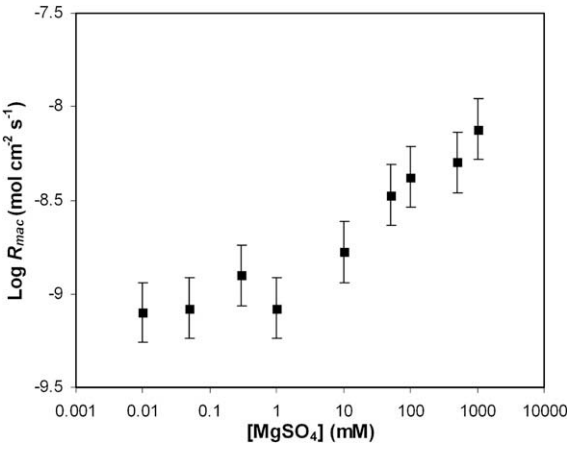

Fig. 9. Macroscopic dissolution rates (R_{mac}) vs. concentration of $MgSO_4$ (rates derived from ICP-OES analyses of total $[Ca^{2+}]$ in effluent solution after 20 min AFM dissolution experiments).

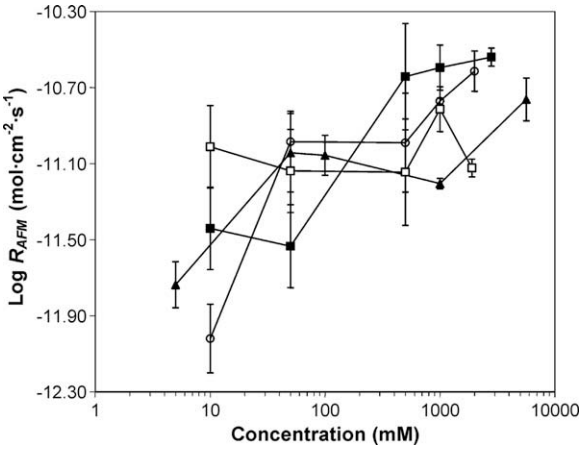

Fig. 10. AFM-derived calcite dissolution rates (R_{AFM}) in saline solutions at neutral pH. Legend: magnesium sulfate (■); magnesium chloride (○); sodium sulfate (□); sodium chloride (▲).

3.5. Crystallite size

Dissolution in water and 2.9 M $MgSO_4$ led to a significant increase in crystallite size determined from broadening of the calcite 104 Bragg peak. The average crystallite size for untreated calcite was 101 ± 5 nm. Following dissolution in deionized water, a 53% increase in crystallite size (up to 155 ± 2 nm) was observed. A 20% increase in crystallite size (up to 121 ± 16 nm) was observed in the case of calcite crystals subjected to dissolution in 2.9 M $MgSO_4$. Finally, no newly-formed (magnesium) phases were detected by XRD.

3.6. ESEM-EDS analysis

Fig. 11 shows representative back scattered electron (BSE) images of the surface of calcite samples subjected to dissolution in water (Fig. 11a) and 2.8 M $MgSO_4$ solution (Fig. 11b). Large terraces limited by jagged steps were developed in the presence of water, while deep etch pits (density ~10^6 cm^{-2}) with rounded +/+ corners were observed in calcite samples subjected to dissolution in magnesium sulfate solution. Note that shallow pits (observed with the AFM) could not be resolved with the ESEM. Otherwise, these observations are fully consistent with AFM results. EDS analyses of the different areas of the etch pits as well as the surface terraces did not allow detection of

Table 3
AFM derived calcite dissolution rates (mol cm^{-2} s^{-1}) for the different salt tested.

NaCl			Na_2SO_4			$MgSO_4$			$MgCl_2$		
(mM)	Log rate	Std	(mM)	Log rate	Std	(mM)	Log rate	Std	(mM)	Log rate	Std
0				−11.75	0.18						
5	−11.74	0.12	10	−11.01	0.10	10	−11.44	0.22	10	−12.02	0.18
50	−11.04	0.21	50	−11.14	0.08	50	−11.53	0.22	50	−10.98	0.16
100	−11.06	0.11	500	−11.14	0.10	500	−10.64	0.28	500	−10.99	0.26
1000	−11.20	0.03	1000	−10.81	0.29	1000	−10.59	0.12	1000	−10.77	0.02
5640	−10.76	0.11	1900	−11.12	0.18	2800	−10.54	0.05	2000	−10.61	0.11

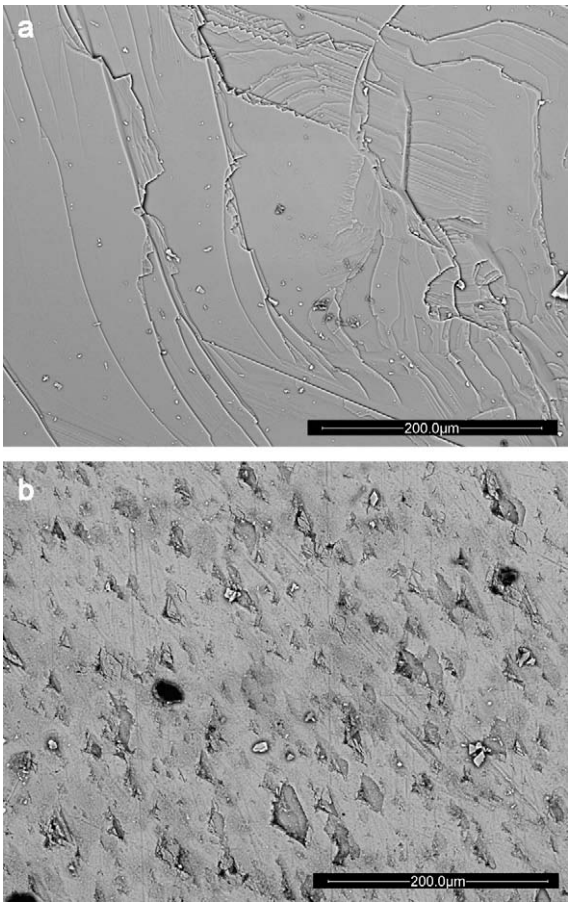

Fig. 11. ESEM backscattered electron photomicrographs of Iceland spar crystals (cleavage plane) subjected to dissolution in flowing (20 min) (a) deionized water and (b) 2.9 M $MgSO_4$ solution.

any magnesium in the sample subjected to dissolution in saturated magnesium sulfate solution.

4. DISCUSSION

Our results show that Mg^{2+} in concentration higher than ~50 mM enhances calcite dissolution. To a lesser extent, Na^+ also promotes calcite dissolution when present in high concentration.

Enhanced dissolution of calcite in the presence of foreign ions could be ascribed to the so-called ionic strength (IS) effect (Buhmann and Dreybrodt, 1987) which leads to a reduction in ion activity coefficients, thus reducing Ω. According to the kinetic theory for calcite dissolution, a reduction in Ω should increase the dissolution rate R ($R = k(1-\Omega)^n$, where k is the rate constant and n is the reaction order (Morse and Arvidson, 2002)). In our experiments, the release of a limited amount of Ca^{2+} and CO_3^{2+} in the AFM cell following calcite dissolution precludes maintenance of a constant Ω equal to 0. However, the concentration of these ions in the cell should be extremely low due to the high flow rate we have used. Therefore, changes in the undersaturation of the system due to an increase in IS are not expected to be significant. The ionic strength also appears to affect the value of k, although there are contradicting results regarding this effect: while Buhmann and Dreybrodt (1987) report that an increase in IS leads to an increase in R, Gledhill and Morse (2006a) report the opposite, and Pokrovsky et al. (2005) report no effect of IS on calcite dissolution rates (up to 1 M NaCl). In any case, dissolution rates are quite different in Na_2SO_4 and $MgCl_2$ solutions (with the exception of 1 M concentration) despite the fact that IS values of these solutions are nearly identical (Table 1). Similarly, sodium and magnesium sulfate solutions have very similar IS values for concentrations $\leqslant$1 M (Table 1), but their dissolution rates are very different (Fig. 10). It follows that the observed enhancement of calcite dissolution can not be explained solely by an increase in IS.

Another possibility for enhanced calcite dissolution would be surface precipitation of newly-formed phases with a higher solubility than calcite. However, direct precipitation of magnesite (or hydromagnesite) or nahcolite is not predicted by our SI calculation, as all systems (with the exception of the saturated $MgCl_2$ solution that shows a $SI_{magnesite}$ of 0.1 and a $SI_{hydromagnesite}$ of 0.18) are undersaturated with respect to these phases (Fig. 1 and Table 1). This is in agreement with the failure to detect the growth of new phases with AFM, XRD and SEM-EDS. In particular, the formation of a Mg-calcite phase which would have lead either to a broadening of the 104 Bragg peak or the appearance of a new peak at a d-spacing smaller than 3.03 Å, is not observed.

It follows that other effects must be responsible for the increase in dissolution rates of calcite in concentrated saline solutions, especially in those containing Mg^{2+}. Such effects appear to be related to the observed nanoscale features of calcite dissolution in the presence of foreign ions, Mg^{2+} in particular, as will be discussed in the following sections.

4.1. Effect of Mg^{2+} on calcite dissolution rates: etch pit spreading vs. deepening rates and etch pit density

Overall, our v_{sum} and etch pit density measurements are in good agreement with those reported by Arvidson et al. (2006). The authors state that Mg^{2+} (in concentration below 0.8 mmolal) inhibits calcite dissolution via reduction of etch pit spreading rate. The authors also report that magnesium significantly increases etch pit density, as observed here. However, Arvidson et al. (2006) do not mention any increase in etch pit depth. This is probably because the maximum magnesium concentration they used was about the threshold for the detection of any significant increase in the depth of etch pits, which in our experiments was found to be 0.3 mM. Apparently, etch pit spreading rate does not seem to be the key for understanding calcite dissolution rates in the presence of $[Mg^{2+}] > 50$ mM. Our R_{AFM} measurements show that in order to fully understand the kinetics of calcite dissolution in the presence of Mg^{2+}, it is necessary to consider both etch pit spreading and deepening rates, as well as etch pit density. In fact, introduction of a correction term, x_A in Eq. (1) accounting for the fractional area occupied by etch pits (i.e., etch pits density, which in turn is proportional to the step density) is critical to evaluate the role of Mg^{2+} in calcite dissolution kinetics. When all these factors are taken into account, the trend in R_{AFM} values confirms that magnesium in concentrations below ~50 mM inhibits calcite dissolution while at higher concentrations dissolution is promoted. Such a promotion at high Mg^{2+} concentration is also consistent with R_{mac} values (despite the errors associated with such measurements, as previously indicated).

Inhibition, which is a maximum in the presence of 10 mM $MgCl_2$ (e.g., $\log R_{AFM} = -12.02(\pm 0.18)$ mol cm^{-2} s^{-1}), is brought about by the reduction in v_+ in conditions where etch pit densities do not reach a threshold value of $\sim 5 \times 10^8$ cm^{-2}. Above this value, corresponding to $[Mg^{2+}] \geqslant 10$–50 mM, the step density is sufficiently high to enhance dissolution (increasing R_{AFM} values) despite the observed reduction in v_{sum} (associated with the reduction in v_+).

4.2. Etch pit nucleation: the possible role of Mg^{2+} adsorption

Etch pit nucleation is a fundamental step in the dissolution of calcite because it provides a source of kinks and step edges that energetically favor the detachment of ions from an otherwise atomically flat surface (Liang et al., 1996). MacInnis and Brantley (1992) have shown that etch pit nucleation on the cleavage face of Iceland spar primarily occurs at defects. This is consistent with our XRD results showing a significant increase in crystallite size following dissolution. Such an increase in crystallite size is consistent with the annihilation of defects outcropping at the calcite surface exposed to the solutions. However, the typical (maximum) value of dislocation density for unstrained Iceland spar is $\sim 10^6$ cm^{-2} (see Bisschop et al., 2006, and refs. therein), a value consistent with the density of deep etch pits observed here using AFM and ESEM. The average density of point defects of Iceland spar is estimated to be $\sim 10^5$ cm^{-2} (MacInnis and Brantley, 1992). The minimum value of etch pit density observed here is 1.8×10^8 cm^{-2} (dissolution in deionized water), a value two orders of magnitude higher than the estimated total defect density and in good agreement with the value of etch pit density ($\sim 10^8$ cm^{-2}) reported by Teng (2004) for Iceland spar dissolution at very low Ω. According to Teng (2004), this shows that in addition to defect-assisted etch pit formation (i.e., deep and shallow pits originated at line and point defects, respectively), a significant amount of the observed etch pits should have originated via unassisted 2D nucleation. In fact, Teng (2004) reports that once $\Omega \leqslant 0.007$, the reduction in the energy barrier for unassisted pit nucleation is sufficient to enable 2D nucleation on defect-free surfaces. Interestingly, in the presence of high Mg^{2+} concentrations we have observed etch pit densities of up to 2.5×10^9 cm^{-2} (i.e., one order of magnitude higher than those reached in deionized water, or NaCl and Na_2SO_4 solutions). Note, however, that the saturation state was extremely low ($\Omega \to 0$) in all our runs. If conditions for unassisted 2D nucleation were the controlling factors in all our dissolution experiments (according to Teng's model), why does enhanced pit nucleation occur in the presence of Mg^{2+}?

The previous effects could be interpreted in terms of Mg^{2+} adsorption (physisorption) onto defect-free calcite surfaces and subsequent competition for hydration water between this ion and the water adsorbed onto the calcite surface (Arvidson et al., 2006; Vinson et al., 2007). Molecular dynamics (MD) simulation by Kerisit and Parker (2004) has shown that Mg^{2+} is able to attract water molecules from the calcite surface to retain a full coordination shell (i.e., 6 water molecules) once it adsorbs as an inner-sphere complex directly above a surface carbonate group. As a result, water molecules could be transferred from surface calcium during magnesium adsorption. This is consistent with MD calculations showing that the residence time of a water molecule in the Mg^{2+} primary hydration shell ($\approx 2.8 \times 10^{-6}$ s) is several orders of magnitude higher than that of Ca^{2+} ($\approx 38 \times 10^{-12}$ s) (Kerisit and Parker, 2004). Such a strong magnesium–surface interaction and the fact that magnesium can disrupt the surface hydration layer can lead to surface destabilization, and ultimately favor 2D nucleation of etch pits. A similar effect is suggested by Vinson et al. (2007) to explain enhanced calcite dissolution in the presence of Mn^{2+}, a cation with a hydration enthalpy (-1845 kJ mol^{-1}) slightly smaller than that of Mg^{2+} (-1921 kJ mol^{-1}) but about 14% greater than that of Ca^{2+} (-1592 kJ mol^{-1}) (Phillips and Williams, 1965). Arvidson et al. (2006) also suggest that the differences in hydration enthalpy between Mg^{2+} and Ca^{2+} ions may explain why enhanced etch pit nucleation occurs in the presence of the former ion. The authors argue (based on MD results by Kerisit and Parker, 2004) that because adsorbed Mg^{2+} bonds to an oxygen from the surface carbonate group, it may leave the calcite surface *with* the carbonate oxygen upon desorption, or its surface detachment could destabilize the surface hydration layer, providing a mechanistic opportunity for subsequent detachment of lattice ions at defect sites. However, Kerisit and Parker (2004) have shown that Mg^{2+} is predicted to stay adsorbed on the sur-

face of calcite for much longer (μs) than Ca^{2+} (ns), thus desorption will not be favored. We suggest that the surface destabilization associated with the disruption of the calcite surface hydration layer brought about by Mg^{2+} adsorption may be enough (without the need of desorption) to reduce the energy barrier for 2D nucleation of a pit. According to the model presented by Dove et al. (2005) for enhanced mineral dissolution in the presence of foreign ions in solution (e.g., soluble salts), adsorption of such ions at the mineral-solution interface favors homogeneous 2D nucleation either by a reduction of the step edge free energy associated with the free energy barrier to stabilizing a pit, or a reduction in the kinetic barrier to removing atoms from the surface to initiate a pit, which manifest itself in the density of nucleation sites. The first hypothesis, i.e., reduction of the step edge free energy associated with the free energy barrier to stabilizing a pit, is not consistent with our observation of unassisted 2D nucleation in the absence of Mg^{2+} (e.g., deionized water runs). In other words, such an energy barrier was already overcome because homogeneous nucleation of etch pit occurs irrespectively of the presence of magnesium due to the low value of Ω in our experiments. Most probably, a reduction in the kinetic barrier associated with the magnesium–calcite surface interaction as described above, initiates etch pit nucleation which in fact manifest itself in an increase (of one order of magnitude) in etch pit density. Such an increase in etch pit nucleation density (and the resulting increase in step density) would lead to the observed increase in the dissolution rate of calcite in the presence of Mg^{2+} ions.

4.3. Magnesium incorporation at $<\bar{4}41>_+$ steps

As previously stated, Mg^{2+} induces a significant reduction in v_+. This is consistent with the reported inhibition effect of magnesium in calcite dissolution (Arvidson et al., 2006). This effect, which is present up to the maximum magnesium concentration used here, is surpassed by the dissolution promotion effect discussed in Section 4.2 (for $[Mg^{2+}] > 50$ mM). Arvidson et al. (2006) suggest that magnesium incorporation at + step edges could explain such an inhibition effect. Note that as opposed to physisorption, incorporation will involve irreversible chemisorption of Mg^{2+} ions into the calcite structure. Site-specific Mg^{2+} incorporation into calcite during growth experiments has been thoroughly described (e.g., Paquette and Reeder, 1995; Davis et al., 2004). However, Mg^{2+} incorporation during calcite dissolution is not well understood (Arvidson et al., 2006). Our AFM observations suggest that site-specific Mg^{2+} incorporation into +/+ corners occurs, thus resulting in the observed reduction of v_+ and the rounding of +/+ corners. In our case, changes in etch pit morphology were not associated with impurities naturally present in Iceland spar crystals (Harstad and Stipp, 2007), otherwise such rounded corners would have been observed in the absence of Mg^{2+} in solution (i.e., dissolution runs with deionized water or $NaCl/Na_2SO_4$ solutions). Arvidson et al. (2006) also report a significant reduction of v_+ and rounding of +/+ corners following dissolution of calcite in the presence of Mg^{2+}. However, this effect was only observed in carbonated solutions (with $[CO_3^{2-}] \sim 10^{-4}$ molal). In the so-called "carbonate-free" solutions the authors observed no change in pit morphology or in the rate of step retreat. Interestingly, Lea et al. (2001) have shown that carbonate ions tend to incorporate into $<\bar{4}41>_+$ steps, leading to their rounding. The authors observed a systematic rounding of the +/+ etch pit corner following addition of Ca^{2+}, Mn^{2+} and Sr^{2+} to carbonated solutions. They concluded that site-specific incorporation of neutral $MeCO_3^\circ$ ion pairs (where Me stands for divalent metal cations) at $<\bar{4}41>_+$ step edges was responsible for the rounding of the +/+ corners. Direct incorporation of Me^{2+} was ruled out based on the poor fit of the terrace-ledge-kink (TLK) model to normalized v_+ using the sum of metal cation activities. An excellent fit was however observed following TLK model fitting to normalized v_+ using the sum of neutral ion-pair. Vinson et al. (2007) have also observed rounding of calcite +/+ etch pit corners upon addition of Mn^{2+} to carbonated solutions. This resulted in a strong inhibition of calcite dissolution. In contrast, the authors observed no such corner rounding in carbonate-free solutions upon Mn^{2+} addition (up to 2×10^{-6} molal manganese). In this latter case, a weak dissolution promotion was observed. The authors suggest that incorporation of $MnCO_3^\circ$ ion-pair at the $<\bar{4}41>_+$ steps may account for the corner rounding and the observed inhibition. They use the surface complexation model (Van Cappellen et al., 1993) to explain $MnCO_3^\circ$ incorporation by the following reaction:

$$> CaOH_2^+ + MnCO_3^\circ \Rightarrow > CaCO_3Mn^+ + H_2O \quad (3)$$

Vinson et al. (2007) argue that formation of the metal carbonate ion-pairs in solution would involve the loss of at least some water molecules from the cations' first hydration shell. This will in turn reduce the energy penalty involved in surface attachment at kink/ledges of $<\bar{4}41>_+$ steps.

A similar process may be at work in our system for the case of Mg^{2+} incorporation into $<\bar{4}41>_+$ steps. Our calculation of ion species distribution show that the activity of $MgCO_3^\circ$ ranges from 10^{-13} M (0.1 mM $MgCl_2$ or $MgSO_4$) up to 10^{-7} M (2.9 M $MgSO_4$) or 10^{-5} M (2 M $MgCl_2$) (Table 1 and Fig. 1). The higher $MgCO_3^\circ$ concentration in $MgCl_2$ solutions, if compared with $MgSO_4$ solutions, may help explain why a more significant rounding of +/+ corners and lower R_{AFM} values were observed in the former solution. Note, however, that the average v_+/v_- ratio of 0.32 ± 0.08 observed here in the presence of Mg^{2+} is much higher than that (0.05 ± 0.04) measured by Arvidson et al. (2006). This is consistent with the higher concentration of $MgCO_3^\circ$ (between 10^{-6} and 10^{-4} M) in the dissolution experiment of these authors. Lea et al. (2001) have calculated that a significant reduction in v_+ (leading to rounding of +/+ corners) occurs when the activity of $MeCO_3^\circ$ is above $\sim 10^{-7}$ M, a value which is reached in our concentrated $MgSO_4$ solutions, and surpassed in the $MgCl_2$ solutions, but is a few orders of magnitude higher than that observed here for the initial reduction of v_+ and corner rounding (i.e., a $MgCO_3^\circ$ activity as low as 10^{-10} M). Apparently, $MgCO_3^\circ$ is much more effective in reducing v_+ than the ion pairs studied by Lea et al. (2001) (i.e.,

$CaCO_3^\circ$, $MnCO_3^\circ$, and $SrCO_3^\circ$), possibly due to the higher affinity of magnesium to be incorporated into + steps of calcite (de Leeuw, 2002).

Molecular dynamics (MD) modeling has shown that Mg^{2+} incorporation into step edges of calcite (as a magnesite layer) is energetically favored in solution with both calcium and magnesium (de Leeuw and Parker, 2001). Furthermore, MD simulation by de Leeuw (2002) shows that only a few rows of Mg^{2+} will be incorporated at steps edges (further incorporation is not energetically favorable). According to the author, such a few rows are sufficient to inhibit growth. Formation of a few atomic layers of magnesite could significantly hamper etch pit spreading rates because its dissolution rate is orders of magnitude lower that that of calcite (i.e., $R_{magnesite} \approx 10^{-14}$ mol cm^{-2} s^{-1}, at circum-neutral pH; Pokrovsky and Schott, 1999). The presence of only a few molecular layers of magnesite formed at calcite step edges may explain why we were not able to detect any magnesium by means of EDS microanalysis (i.e., magnesium concentration should be below the detection limit of EDS, which is about a few hundred ppm (Reed, 1996)). Cicerone et al. (1992), based on electrokinetic measurements of the calcite/water interface in the presence of magnesium ions, suggest the possible formation of a magnesium-bearing calcite. However, formation of a Mg-calcite layer would not led to a reduction in the etch pit spreading rate because Mg-calcites are reported to have dissolution rates nearly equal, or even slightly higher than that of calcite (Walter and Morse, 1985).

As etch pits cannot spread due to blocking by Mg^{2+}, dissolution takes place by means of the formation of new pits. Once the surface is covered by etch pits, the dissolution continues with the formation of successive etch pits (narrower) within preexisting ones via the mechanism described in Section 4.2. Conversely, etch pits deepening could progress along deep dislocations as shown in Fig. 6. These two processes enable the advancement of the dissolution front normal to $\{10\bar{1}4\}$ surfaces, thus promoting calcite dissolution despite the observed inhibition of etch pit spreading.

4.4. The role of SO_4^{2-} in magnesium-induced calcite dissolution

It is known that the rate limiting step for Mg^{2+} adsorption and incorporation into carbonates is its dehydration (Lippmann, 1973). Sulfates are known to enhance cation desolvation through the formation of ion pairs (Piana et al., 2006). In $MgSO_4$ solutions, Mg^{2+} and SO_4^{2-} hydrated ions combine to form double solvent separated ion pairs. Initially, such ion pairs have a number of hydration shells similar to that of free Mg^{2+} and SO_4^{2-} ions. As concentration increases, water molecules are lost from such complexes to form solvent-shared contact ion pairs (Buchner et al., 2004). Apart from these 1:1 ion pairs, higher order ions (triple or quadruple ion species) appear at concentrations above 1 M. Overall, magnesium adsorption should increase with ion-pair concentration in solution. In this respect, Brady et al. (1996) have shown that adsorption of magnesium on carbonates is enhanced in sulfate-rich solutions. As previously discussed in Section 4.2, Mg^{2+} adsorption could enhance calcite dissolution. Although etch pit spreading rates were reduced in the presence of both $MgSO_4$ and $MgCl_2$, etch pit deepening rates were much higher in the presence of SO_4^{2-} than in the presence of Cl^-. This also holds true for the rates of dissolution (Fig. 10). Moreover, etch pit densities were higher in the presence of sulfates than in their absence (Fig. 4), an observation which is consistent with an increase in Mg-adsorption leading to enhanced etch pit nucleation resulting in an increase in dissolution rates.

4.5. The role of Na^+ in calcite dissolution

Dissolution rates are significantly increased in concentrated NaCl and Na_2SO_4 solutions. As has been previously indicated, changes in IS may affect the dissolution rate R (independently from variations in activity coefficients) by changing the value of k. However, R_{AFM} of NaCl and Na_2SO_4 solutions with equal IS are different. For instance, 5.7 M NaCl solutions with an IS of 5.7, equal to that of 1.9 M Na_2SO_4, have R_{AFM} values of $10^{-10.76}$ and $10^{-11.12}$ mol cm^{-2} s^{-1}, respectively. Because an increase in IS does not seem to explain our results, we have explored the possible interaction of Na^+ ions with the calcite surface as a way to understand why these ions increase calcite dissolution rates. The low hydration enthalpy of Na^+ (-406 kJ mol^{-1}) would not favor enhanced 2D nucleation following adsorption onto calcite, as in the case of Mg^{2+}. In fact, etch pit densities in the presence of Na^+ were very similar to those of deionized water (for the whole range of Na^+ concentrations). Moreover, on the basis of electrostatic considerations, monovalent cations should adsorb less strongly than divalent ones, and their adsorption would only be important when present at very high concentration, as has been reported for cation adsorption on dolomite surfaces (Brady et al., 1996). In our experiments, enhanced calcite dissolution is clearly related to the increase in v_{sum} observed at high Na^+ concentrations. It is however unclear how such an increase in v_{sum} up to a value of 5.5 nm s^{-1} (about three times higher than that of deionized water) occurs. We suggest that Na^+ adsorption at active sites (kinks and/or step edges) may reduce the step edge free energy (Dove et al., 2005) leading to faster step retreat and enhanced dissolution.

5. CONCLUSIONS

The use of *in situ* AFM enables the interpretation of calcite dissolution in the presence of Mg^{2+} at high ionic strengths. Calcite dissolution is enhanced in the presence of solutions containing alkali and alkaline-earth cations, especially in the case of Mg^{2+}. Although previous papers have indicated that Mg^{2+} plays a role as inhibitor of calcite dissolution at pH of ~7 (Arvidson et al., 2006), our results show that at high ionic strengths calcite dissolves faster and the amount dissolved increases with Mg^{2+} concentration. As reported for other minerals such as quartz (Dove et al., 2005), this seems to be mainly due to the interaction between cations and mineral surfaces. Mg^{2+} blocks calcite

etch pit spreading by its preferential incorporation as $MgCO_3^\circ$ at kink/step sites in +/+ corners, possibly through surface reaction with $>CaOH_2^+$ sites. The formation (of a few rows) of $MgCO_3$ at + steps may significantly reduce etch pit spreading rates (via reduction of v_+) because the dissolution rate of such a phase is orders of magnitude lower than that of calcite. Mg^{2+} adsorption fosters etch pit nucleation both at terraces and within existing etch pits and, hence, the dissolution process advances normal to the surface exposed to the solution increasing the dissolution rate. Enhanced dissolution in the presence of Na^+ may be explained by adsorption of this ion at steps, thereby reducing the step edge free energy and increasing v_{sum}. The overall dissolution process is enhanced by high sulfate concentrations, because these anions could enhance Mg^{2+} ions adsorption by fostering their dehydration, thereby promoting etch pit nucleation. In conclusion, as shown in this paper, Mg^{2+} does inhibit the etch pit spreading rate on calcite surfaces, but this parameter alone is not indicative of the overall dissolution rate, which in fact is augmented in the presence of both Mg^{2+} and Na^+ ions.

These results may help understand the significant enhancement of chemical weathering rates associated with saline waters in contact with carbonate rock outcrops (Threnhaile, 1987) as well as the observed enhanced dissolution of calcitic ornamental stone when in contact with Mg-rich solutions (associated with epsomite salts) often present within rock pores (Ruiz-Agudo, 2007; Ruiz-Agudo et al., 2007).

ACKNOWLEDGMENTS

This work has been financially supported by the European Commission VIth Framework Program, under Contract No. SSP1-CT-2003-501571 and the Spanish government under Contract MAT2006-00578. Financial support has also been provided by the research group NRM-179 (Junta de Andalucía, Spain). The research at Münster University is supported by the Deutsche Forschungsgemeinschaft (DFG). The authors thank Dr. Arvidson, Dr. Oelkers, and two anonymous reviewers for their comments and suggestions that helped improve an earlier draft of this paper.

REFERENCES

Alkattan M., Oelkers E. H., Dandurand J. L. and Schott J. (2002) An experimental study of calcite dissolution rates at acidic conditions and 25 °C in the presence of $NaPO_3$ and $MgCl_2$. *Chem. Geol.* **190**, 291–302.

Arvidson R. S., Ertan I. E., Amonette J. E. and Luttge A. (2003) Variations in calcite dissolution rates: a fundamental problem?. *Geochim. Cosmochim. Acta* **67** 1623–1624.

Arvidson R. S., Collier M., Davis K. J., Vinson M. D., Amonette J. E. and Luttge A. (2006) Magnesium inhibition of calcite dissolution kinetics. *Geochim. Cosmochim. Acta* **70**, 583–594.

Astilleros J. M., Pina C. M., Fernández-Díaz L., Prieto M. and Putnis A. (2006) Nanoscale phenomena during the growth of solid solutions on calcite $\{1\,0\,\bar{1}\,4\}$ surfaces. *Chem. Geol.* **225**, 322–335.

Barwise A. J., Compton R. G. and Unwin P. R. (1990) The effect of carboxylic acids on the dissolution of calcite in aqueous solution. Part 2.—D-,L- and meso-tartaric acids. *J. Chem. Soc. Faraday Trans.* **86**, 137–144.

Bearat H., McKelvy M. J., Chizmeshya A. V., Gormley D., Nunez R., Carpenter R. W., Squires K. and Wolf G. H. (2006) Carbon sequestration via aqueous olivine mineral carbonation: role of passivating layer formation. *Environ. Sci. Technol.* **40**, 4802–4808.

Bell F. G. (1993) Durability of carbonate rock as building stone with comments on its preservation. *Environ. Geol.* **21**, 187–200.

Berner R. A. (1967) Comparative dissolution characteristics of carbonate minerals in the presence and absence of aqueous magnesium. *Am. J. Sci.* **265**, 45–70.

Bisschop J., Dysthe D. K., Putnis C. V. and Jamtveit B. (2006) In situ AFM study of the dissolution and recrystallization behaviour of polished and stressed calcite surfaces. *Geochim. Cosmochim. Acta* **70**, 1728–1738.

Brady P. V., Krumhansl J. L. and Papenguth H. W. (1996) Surface complexation clues to dolomite growth. *Geochim. Cosmochim. Acta* **60**, 727–731.

Buchner R., Chen T. and Hefter G. (2004) Complexity in simple electrolyte solutions: ion pairing in $MgSO_4$(aq). *J. Phys. Chem. B* **108**, 2365–2375.

Buhmann D. and Dreybrodt W. (1987) Calcite dissolution kinetics in the system H_2O–CO_2–$CaCO_3$ with participation of foreign ions. *Chem. Geol.* **64**, 89–102.

Cicerone D. S., Regazzoni A. E. and Blesa M. A. (1992) Electrokinetic properties of the calcite/water interface in the presence of magnesium and organic matter. *J. Colloid Interface Sci.* **154**, 423–433.

Compton R. G. and Brown C. A. (1994) The inhibition of calcite dissolution/precipitation: Mg^{2+} cations. *J. Colloid Interface Sci.* **165**, 445–449.

Davis J. A., Fuller C. and Cook A. D. (1987) A model for trace metal sorption processes at the calcite surface: adsorption of Cd^{2+} and subsequent solid solution formation. *Geochim. Chosmochim. Acta* **51**, 1477–1490.

Davis K. J., Dove P. M. and De Yoreo J. J. (2000) The role of Mg^{2+} as an impurity in calcite growth. *Science* **290**, 1134–1137.

Davis K. J., Dove P. M., Wasylenki L. E. and De Yoreo J. J. (2004) Morphological consequences of differential Mg^{2+} incorporation at structurally distinct steps on calcite. *Am. Mineral.* **89**, 714–720.

De Giudici G. (2002) Surface control vs. diffusion control during calcite dissolution: dependence of step-edge velocity upon solution pH. *Am. Mineral.* **87**, 1279–1285.

de Leeuw N. H. and Parker S. C. (2001) Surface–water interactions in the dolomite problem. *Phys. Chem. Chem. Phys.* **3**, 3217–3221.

de Leeuw N. H. (2002) Molecular dynamics simulation of the growth inhibition effect of Fe^{2+}, Mg^{2+}, Cd^{2+}, and Sr^{2+} on calcite crystal growth. *J. Phys. Chem. B* **106**, 5241–5249.

Dove P. M. and Platt F. M. (1996) Compatible real-time rates of minerals dissolution by Atomic Force Microscopy (AFM). *Chem. Geol.* **127**, 331–338.

Dove P. M., Han N. and De Yoreo J. J. (2005) Mechanisms of classical crystal growth theory explain quartz and silicate dissolution behavior. *Proc. Natl. Acad. Sci. USA* **102**, 15357–15362.

Drever J. I. (1997) *The Geochemistry of Natural Waters. Surface and Groundwater Environments*, third ed. Prentice-Hall, NJ.

Duckworth O. W. and Martin S. T. (2004) Dissolution rates and pit morphologies of rhombohedral carbonate minerals. *Am. Mineral.* **89**, 554–563.

El-Korashy S. A. (2003) Studies on divalent ion uptake of transition metal cations by calcite through crystallization and cation exchange process. *J. Mater. Sci.* **38**, 1709–1719.

García-Sánchez A. and Álvarez-Ayuso E. (2002) Sorption of Zn, Cd and C on calcite. Application to purification of industrial wastewaters. *Minerals Eng.* **15**, 539–547.

Gledhill D. K. and Morse J. W. (2006a) Calcite dissolution kinetics in Na–Ca–Mg–Cl brines. *Geochim. Cosmochim. Acta* **70**, 5802–5813.

Gledhill D. K. and Morse J. W. (2006b) Calcite solubility in Na–Ca–Mg–Cl brines. *Chem. Geol.* **233**, 249–256.

Goudie A. and Viles H. (1997) *Salt Weathering Hazards*. Wiley, Chichester.

Hall C. and Cullen D. C. (1995) Scanning force microscopy of gypsum dissolution and crystal growth. *AIChE J.* **42**, 232–238.

Hanor J. S. (1994) Physical and chemical controls on the composition of waters in sedimentary basins. *Mar. Petrol. Geol.* **11**, 31–45.

Harstad A. O. and Stipp S. L. S. (2007) Calcite dissolution: effects of trace cations naturally present in Iceland spar calcites. *Geochim. Cosmochim. Acta* **71**, 56–70.

Hay M. B., Workman R. K. and Manne S. (2003) Mechanisms of metal ion sorption on calcite: composition mapping by lateral force microscopy. *Langmuir* **19**, 3727–3740.

He S. and Morse J. W. (1993) Prediction of halite, gypsum, and anhydrite solubility in natural brines under subsurface conditions. *Comput. Geosci.* **19**, 1.

Hillner P. E., Gratz A. J., Manne S. and Hansma P. K. (1992) Atomic scale imaging of calcite growth and dissolution in real time. *Geology* **20**, 359–362.

Jordan G. and Rammensee W. (1997) Growth and dissolution on the CaF_2 (1 1 1) surface observed by scanning force microscopy. *Surf. Sci.* **371**, 371–380.

Jordan G. and Rammensee W. (1998) Dissolution rates of calcite ($1\,0\,\bar{1}\,4$) obtained by scanning force microscopy: microtopography-based dissolution kinetics on surfaces with anisotropic step velocities. *Geochim. Cosmochim. Acta* **62**, 941–947.

Kanellopoulou D. G. and Koutsoukos P. G. (2003) The calcitic marble/water interface. Kinetics of dissolution and inhibition with potential implications in stone conservation. *Langmuir* **19**, 5691–5699.

Kerisit S. and Parker S. C. (2004) Free energy of adsorption of water and metal ions on the $\{1\,0\,\bar{1}\,4\}$ calcite surface. *J. Am. Chem. Soc.* **126**, 10152–10162.

Lea A. S., Amonette J. E., Baer D. R., Liang Y. and Colton N. G. (2001) Microscopic effects of carbonate, manganese and strontium ions on calcite dissolution. *Geochim. Cosmochim. Acta* **65**, 369–379.

Liang Y., Baer D. R., McCoy J. M., Amonette J. E. and LaFemina J. P. (1996) Dissolution kinetics at the calcite–water interface. *Geochim. Cosmochim. Acta* **60**, 4883–4887.

Liang Y. and Baer D. R. (1997) Anisotropic dissolution at the $CaCO_3$ ($1\,0\,\bar{1}\,4$)–water interface. *Surf. Sci.* **373**, 275–287.

Lippmann F. (1973) *Sedimentary Carbonate Minerals*. Springer-Verlag, Berlin.

MacInnis I. N. and Brantley S. L. (1992) The role of dislocations and surface morphology in calcite dissolution. *Geochim. Cosmochim. Acta* **56**, 1113–1126.

Mann S. (2001) *Biomineralization: Principles and Concepts in Bioinorganic Materials Chemistry*. Oxford University Press, Oxford.

Martin-Ramos D. (2004) XPowder: A Software Package for Powder X-Ray Diffraction Analysis, Version 2004.03. Available from: <www.xpowder.com/>.

Monnin C. and Schott J. (1984) Determination of the solubility products of sodium carbonate minerals and an application to trona deposition in Lake Magadi (Kenya). *Geochim. Cosmochim. Acta* **48**, 571–581.

Morel F. M. M. (1983) *Principles of Aquatic Chemistry*. John Wiley and Sons, New York.

Morse J. W. and Arvidson R. S. (2002) The dissolution kinetics of major sedimentary carbonate minerals. *Earth Sci. Rev.* **58**, 51–84.

O'Connor W. K., Dahlin D. C., Ochs T. L. and Turner P. C. (1999) Process for carbon dioxide sequestration by direct mineral carbonation. U.S. Dept. of Energy: Office of Assistant General Counsel for Patents, Chicago, IL (Record of Invention).

Paquette J. and Reeder R. J. (1995) Relationship between surface structure, growth mechanism, and trace element incorporation in calcite. *Geochim. Cosmochim. Acta* **59**, 735–749.

Parkhurst D. L. and Appelo C. A. J. (1999) Users guide to PHREEQC (version 2) – a computer program for speciation, batch reaction, one dimensional transport, and inverse geochemical calculations. U.S. Geological Survey Water-Resources Investigation Report 99-4259, 312pp.

Phillips C. S. G. and Williams R. J. P. (1965) *Inorganic Chemistry 1*. Oxford University Press, New York.

Piana S., Jones F. and Gale J. D. (2006) Assisted desolvation as a key kinetic step for crystal growth. *J. Am. Chem. Soc.* **128**, 13568–13574.

Pokrovsky O. S. and Schott J. (1999) Processes at the magnesium-bearing carbonates/solution interface. II. Kinetics and mechanism of magnesite dissolution. *Goechim. Cosmochim. Acta* **63**, 881–897.

Pokrovsky O. S., Golubev S. and Schott J. (2005) Dissolution kinetics of calcite, dolomite and magnesite at 25 °C and 0 to 50 atm pCO_2. *Chem. Geol.* **217**, 239–255.

Putnis A., Junta-Rosso J. L. and Hochella, Jr., M. F. (1995) Dissolution of barite by a chelating ligand: an atomic force microscopy study. *Geochim. Cosmochim. Acta* **59**, 4623–4632.

Reed S. J. B. (1996) *Electron Microprobe Analysis and Scanning Electron Microscopy in Geology*. Cambridge University Press, Cambridge.

Ruiz-Agudo E. (2007) Prevención del daño debido a la cristalización de sales en el patrimonio histórico construido mediante el uso de inhibidores de la cristalización. Ph. D. thesis. Universidad de Granada, Granada.

Ruiz-Agudo E., Mees F., Jacobs P. and Rodriguez-Navarro C. (2007) The role of saline solution properties on porous limestone salt weathering by magnesium and sodium sulfates. *Environ. Geol.* **52**, 269–281.

Sabbides G. and Koutsoukos P. G. (1995) Dissolution of calcium carbonate in the presence of magnesium and inorganic orthophosphate. In *Mineral Scale Formation and Inhibition* (ed. Z. Amjad). Plenum Press, New York, pp. 73–86.

Shiraki R., Rock P. A. and Casey W. H. (2000) Dissolution kinetics of calcite in 0.1 M NaCl solution at room temperature: an atomic force microscopic (AFM) study. *Aquat. Geochem.* **6**, 87–108.

Shtukenberg A. G., Astilleros J. M. and Putnis A. (2005) Nanoscale observations of the epitaxial growth of hashemite on barite (0 0 1). *Surf. Sci.* **590**, 212–223.

Sjöberg E. L. (1978) Kinetics and mechanism of calcite dissolution in aqueous solutions at low temperatures. *Stockholm Contrib. Geol.* **32**, 92.

Smith B. J., Warke P. A. and Moses C. A. (2000) Limestone weathering in contemporary arid environments: a case study from southern Tunisia. *Earth Surf. Process. Land.* **25**, 1343–1354.

Teng H. H., Dove P. M., Orme C. and De Yoreo J. J. (1998) Thermodynamics of calcite growth: baseline for understanding biomineral formation. *Science* **282**, 724.

Teng H. H. (2004) Control by saturation state on etch pit formation during calcite dissolution. *Geochim. Cosmochim. Acta* **68**, 253–262.

Trenhaile A. S. (1987) *The Geomorphology of Rock Coasts*. Oxford University Press, Oxford.

Van Cappellen P., Charlet L., Stumm W. and Wersin P. (1993) A surface complexation model of the carbonate mineral–aqueous solution interface. *Geochim. Cosmochim. Acta* **57**, 3505–3518.

Vinson M. D. and Luttge A. (2005) Multiple length-scale kinetics: an integrated study of calcite dissolution rates and strontium inhibition. *Am. J. Sci.* **305**, 119–146.

Vinson M. D., Arvidson R. S. and Luttge A. (2007) Kinetic inhibition of calcite (104) dissolution by aqueous manganese(II). *J. Crystal Growth* **307**, 116–125.

Walter L. M. and Morse J. W. (1985) The dissolution kinetics of shallow marine carbonates in seawater: a laboratory study. *Geochim. Cosmochim. Acta* **49**, 1503–1513.

White A. F. and Brantley S. L. (eds.) (1995) Chemical weathering rates of silicate minerals. In *Reviews in Mineralogy*, vol. 31. Mineralogical Society of America, Washington, DC.

Wolf G. H., Chizmeshya A. V., Diefenbacher J. and McKelvy M. J. E. (2004) In situ observation of CO_2 sequestration reactions using a novel microreaction system. *Environ. Sci. Technol.* **38**, 932–936.

Associate editor: Eric H. Oelkers